EFFICIENT NUMERICAL EVALUATION OF EXACT SOLUTION FOR 1D, 2D AND 3D INFINITE CYLINDRICAL HEAT CONDUCTION PROBLEM

by

Te Pi

A DISSERTATION

Presented to the Faculty of

The Graduate College at the University of Nebraska

In Partial Fulfillment of Requirements

For the Degree of Doctor of Philosophy

Major: Mechanical Engineering & Applied Mechanics

Under the Supervision of Professor Kevin D. Cole

Lincoln, Nebraska

March, 2018

EFFICIENT NUMERICAL EVALUATION OF EXACT SOLUTION FOR 1D, 2D AND 3D INFINITE CYLINDRICAL HEAT CONDUCTION PROBLEM

Te Pi, Ph.D.

University of Nebraska, 2018

Advisor: Kevin D. Cole

Estimation of thermal properties or diffusion properties from transient data requires that a model is available that is physically meaningful and suitably precise. The model must also produce numerical values rapidly enough to accommodate iterative regression, inverse methods, or other estimation procedures during which the model is evaluated again and again. Bodies of infinite extent are a particular challenge from this perspective. Even for exact analytical solutions, because the solution often has the form of an improper integral that must be evaluated numerically, lengthy computer-evaluation time is a challenge. The subject of this thesis is improving the computer evaluation time for exact solutions for infinite and semi-infinite bodies in the cylindrical coordinate system. The motivating applications for the present work include the line-source method for obtaining thermal properties, the estimation of thermal properties by the laser-flash method, and the estimation of aquifer properties or petroleum-field properties from well-test measurements. In this thesis the computer evaluation time is improved by replacing the integral-containing solution by a suitable finite-body series solution. Although the series solution is approximate, the precision of the series solution may be controlled to a high level and the required computer time may be minimized, by a suitable choice of the extent of the finite body. An easy-to-use relationship is developed for the finite-body size needed as a function of desired precision and as a function of time. The method is demonstrated for the one-dimensional case of large body with a cylindrical hole and is extended to two-dimensional and three-dimensional geometries of practical interest. The computer-evaluation time for the finite-body solutions are shown to be hundreds or thousands of time faster than the

infinite-body solutions, depending on the geometry. Future work is considered to apply the same method from the diffusion problem to other geometries problem.

Table of Contents

APPENDIX: TABLES

CHAPTER 1: INTRODUCTION

1.1 Application

Estimation of thermal properties or diffusion properties from transient data requires that a model is available that is physically meaningful and suitably precise. The model must also produce numerical values rapidly enough to accommodate iterative regression, inverse methods, or other estimation procedures during which the model is evaluated again and again. Bodies of infinite extent are a particular challenge from this perspective. Even for exact analytical solutions, because the solution often has the form of an improper integral that must be evaluated numerically, lengthy computer-evaluation time is a challenge. For the case of a large body with a hole which can be also denoted as semi-infinite cylindrical case, its analytical solution with Green's function is well known [1]. This solution contains an integral that covers a range from zero to infinity and has an integrand which contains products of Bessel's function, consequently this calculation is lengthy and inefficient. Study of infinite or semi-infinite domain problem has always been a challenge, most of numerical methods for solving similar problem such as finite element method (FEM) or finite volume method(FVM) can't maintain precision and efficiency at the same time. The purpose of this dissertation is to find a proper approach for substituting an appropriate finite domain into infinite domain while maintaining precision and improving computational efficiency.

There are several important applications for diffusion theory in the cylindrical geometry. For example, in oil and gas exploration, wells are drilled into the ground and affected by the pressure or temperature acting on their boundary. The effect of the pressure and temperature may lead to some damage or fatigue problems on the wall of well. Nadège and Valérie [2] did experiments for testing and modelling of an industrial insulated pipeline for deep sea. Two thermomechanical finite element model of the coated pipeline were developed to predict its behavior during service condition tests. Omidi *et al.* [3] explored modeling and simulation of hydrate thermal dissociation around a gas production pipe. The effect of gas flow velocity in pipes, porosity of sediment layers and thermal conductivity constant in pipes on two important parameters of volume of hydrate and its decomposition pattern were studied in their research. Sun and Wang [4] discussed heat transfer coefficient during heat assembly of aluminum alloy drill pipes.

Liu *et al.* [5] discussed a method of computing the thermal conductivity of heat-insulation oil pipe coupling. Based on their results, the thermal conductivity and the temperature distribution of heat-insulation oil pipe coupling and the temperature distribution of heat-insulation oil pipe can be obtained easily and accurately. Wong-Loyaa *et al.* [6] studied a 3-D wellbore simulator to determine the thermal diffusivity of rock formations. Thermal diffusivities of rock formations were inversely computed by using an iterative and efficient numerical simulation, where simulated thermal recovery data sets were statistically compared with those temperature measurements logged in geothermal wellbores.

The geometry under consideration in the well problem takes the form of a large body with a hole with a first kind of boundary condition and zero initial condition. There are several ways to solve this cylindrical heat conduction problem. Gholamali and Mohammad [7] did some research on analytical solution of the non-Fourier axisymmetric temperature field within a finite hollow cylinder by using the standard method of separation of variables. Laplace transform and inverse Laplace theorem are another method for solving problems with similar geometry. Yeh and Yang [8] worked on a radial two-layer model of a finite-radius well with the Laplace transform method. Some other work related to Laplace transform method for solving cylindrical transient heat conduction problem has been done by Li and Lai [9] and Zhou and Lee [10]. Cheng and Huang [11] presented an analytical transient heat conduction time function for a steam injection technique considering the wellbore heat capacity.

Inverse methods have been used to estimate temperature-dependent thermal properties in cylindrical geometries. Differential scanning calorimetric was used to estimate the specific [12]. Mohammad *et al.* [13] discussed transient inverse heat conduction problem of quenching a hollow cylinder by one row of water jets. The inverse solution method was validated by a set of artificial data and a sensitivity analysis was done to predict the temperature or heat flux on the quenching surface. Liu and Zhou [14] explored the inverting methods for thermal reservoir evaluation of enhanced geothermal system. They developed a three-dimensional fuzzy inverting model which is able to compute the entire geothermal field temperature and establish the quantitative relationship between heat storage quantity and reservoir thermal property.

The line source model is widely used for ground coupled heat pump systems and radial heat transfer cases. Zeng and Diao [15] studied analytical solution of the transient temperature response in a semi-infinite medium with a line source of finite length, which is a more appropriate model for boreholes in geothermal heat exchangers. The borehole wall temperatures, the middle point temperature and the integral mean temperature are defined in their research. Lamarche and Beauchamp [16] propose another analytical model for heat transfer around vertical ground heat exchangers that yields results very similar to published numerical results. This analytical model for geothermal borehole problems offers better flexibility to design the parameter of heat exchanger and evaluate the temperature change in the borehole and in the ground surrounding it.

Numerical Methods are commonly applied to heat conduction problems with irregular geometries and boundary conditions. Such methods are commonly called Computational Fluid Dynamics (CFD). Commercial software package such as Abaqus and ANSYS FLUENT is widely used for solving diffusion problems with cylindrical geometries. Guo and Zhu [17] developed the CFD modeling for transport and reaction in packed bed chemical looping combustion (CLC) reactors, which was modeled as a cylindrical fixed bed randomly packed with porous spheres that represents the oxygen carrier particles. This CFD model provides very detailed fields of flow, temperature and species and their transient evolution in the interstitial void spaces of the reactor and inside the discrete particles. Combined Artificial Neural Network and Genetic Algorithm (ANN–GA) optimization of hollow cylindrical pin fin on a vertical base plate is explored by Balachandar *et al.* [18] by using ANSYS FLUENT. This kind of geometry is seen in laptops and microprocessors in which the electric circuits generate heat while performing work which necessitates the use of fins. Hollow fins provide an increased heat transfer and a weight reduction of about 90% when compared to solid cylindrical pin fins. Convective heat transfer is predicted in disk-type electrical machines [19]. A linear correlation between the surface temperature of the rotor, the stator and the cover is made by averaging the values of fluid temperature adjacent to the corresponding surface so the bulk fluid temperature can be estimated. Numerical modelling of twin-screw pumps is analyzed based on CFD [20]. In this model, the instantaneous mass flow rates, rotor torque, local pressure field velocity field and other performance indicators including the

indicated power were predicted. The performance simulation for heat exchangers can also be explored by using CFD software in half cylindrical space [21]. The influences of geometrical parameters of baffle pitch and projection length of the inclined section on heat transfer and pressure drop were discussed quantitatively.

Another method for solving diffusion problems in the cylindrical geometry is the Green's function method. Clow [22] discussed the thermal disturbance caused by drilling deep boreholes in rock or ice and provided compact analytical solutions for this disturbance based on 1-D (radial) and 2-D (radial and depth) Green's functions in cylindrical coordinates in 3 general boundary conditions. Renterghem *et al.* [23] discussed a method for airborne sound propagation over sea during offshore wind farm piling. Detailed numerical calculations have been performed with the Green's Function Parabolic Equation (GFPE) method to estimate the sound pressure levels under downwind conditions. Brixa *et al.* [24] use Green's Functions to establish models to predict the carbon dioxide changes for the oceanic part in the project of the NASA Carbon Monitoring System. The model sensitivity experiments include simulations that start from different initial conditions as well as experiments that perturb air–sea gas exchange parameters and the ratio of particulate inorganic to organic carbon.

The Green's function has been also applied to biology and medicine area. Thorsten *et al.* [25] derive an exact Green's function of the diffusion equation for a pair of disk-shaped interacting particles in two dimensions subject to a backreaction boundary condition and use the obtained function to describe the reversible membrane-bound reactions in cell biology. Many-body Green's function perturbation theories, such as the GW and Bethe–Salpeter formalisms are used to study excited states properties of organic molecules in chemical physics [26] as well as the polarizable continuum model, which is a state-specific non-equilibrium approach to explore the case of the evolution of the ionization potential of nucleobases from the gas to the aqueous phase. [27]. Computational modeling of a carbon nanotube-based DNA nanosensor is discussed and the sensor's electrical conductance and transmission coefficients are calculated at the equilibrium geometries via the non-equilibrium Green's function scheme [28]. Loze *et al.* [29] discussed the temperature distributions in laser-heated biological tissue using a time-domain method based on Green's functions.

1.2 Number System

In order to express the geometry in this paper more concisely and precisely, the heat conduction number system [30] is used. The number system is used to categorize solutions of the heat (diffusion) equation to make existing solutions easier to identify, store, and retrieve. Here the number system is used to specify the coordinate system and the type of boundary conditions. For example, consider a large body with a hole case shown in Fig 1a, which is denoted by R20: the number R20 denotes heat conduction in cylindrical coordinates (by the R) with a specified-flux (Neumann) boundary condition at r=R1 (by the 2 in R20) and no physical boundary at $r \to \infty$ (by the 0 in R20); As another example, number R22 denotes heat conduction in the hollow cylinder with a specified heat flux at $r=R_1$ (by the 2 in R22) and specified heat flux at $r=R_2$ (by the second 2 in R22). For 2D cases in this paper, symbol Z is used to denote the z-direction. Examples in two dimensional models: R20Z22 denotes heat conduction in large body with a hole (by the R20) between two planes (by the Z22); number R22Z22 denotes heat conduction in hollow cylinder (by the R22) between two planes (by the Z22); number R00Z22 denotes heat conduction in the infinite body between two planes and number R02Z22 denotes the finite solid cylinder between two planes case. More details about number system can be found from EXACT Analytical Conduction Toolbox [31].

1.3 Overview

In this thesis, the calculation speed is improved for the exact solution of several heat conduction problems of semi-infinite geometries in cylindrical coordinates. For the one-dimensional problem, the temperature is compared between R20 and R22 case. By varying the location of R22's outer boundary, the outer boundary of R22 can be chosen appropriately to give results in agreement with R20 to 8-9 decimal places. From that, it is possible to compute the R20 case more efficiently by using the R22 case as a replacement. For two-dimensional problems, two different geometries have been selected to make comparison: first is R20Z22 case, which can be described as semi-infinite hollow cylinder of finite axial length; second is R00Z22 case, which can be described as infinite solid cylinder of finite axial length. Three-dimensional cylindrical coordinate cases R20φ00Z22 and R21φ00Z22 are discussed as well. By applying Green's function to solve both cases,

the solution for R20φ00Z22 contains infinite-domain integral and double summation series while for R21φ00Z22, there's triple summation series in its solution.

As in the 1-D case, a large improvement in computational speed is shown by replacing the semi-infinite radial domain by a finite radial domain to maintain precision. For the 2-D cases and 3-D cases, results also show an improvement on efficiency by applying the same idea from the 1-D comparison.

1.4 Nomenclature

a radius of inner cylinder **(*m*)** / length of heating region in R02 & R00 cases ***(m)***

A precision for computing exact solution

b introduced point in integral interval for R20 case and R20Z22 case /radius of outer cylinder in R22Z22 case and R02Z22 case ***(m)***

f initial temperature ***(℃)***

G Green's function for the region $a < r < \infty$ ***(1/m²)***

k thermal conductivity ***(cal/(m sec ℃))***

L height of cylinder ***(m)***

L1 length of heater region in R20Z22 and R22Z22 case ***(m)***

q Heat Flux ***(cal/(m²sec))***

r, r' radial space coordinates **(*m*)**

R Overall radius ***(m)***

R_1 inner radius of R20 and R22 case ***(m)***

R_2 outer radius of R22 case ***(m)***

t time ***(sec)***

T temperature ***(℃)***

T_{in} initial temperature ***(℃)***

z, z' length space coordinates ***(m)***

α thermal diffusivity ***(cm^2/sec)***

ε precision for computation

$\tilde{()}$ dimensionless group

CHAPTER 2: ONE-DIMENSIONAL CASES

2.1 Mathematical model for 1D case R20

In this section, the mathematical model for 1D case R20 will be discussed. As shown in Fig 1a, the region of R20 case is $R_1 < r < \infty$ and the cylinder at r=R_1 has constant heat flux. Figure 1b shows the R22 case has an insulated boundary condition at r=R_2, which will be discussed later.

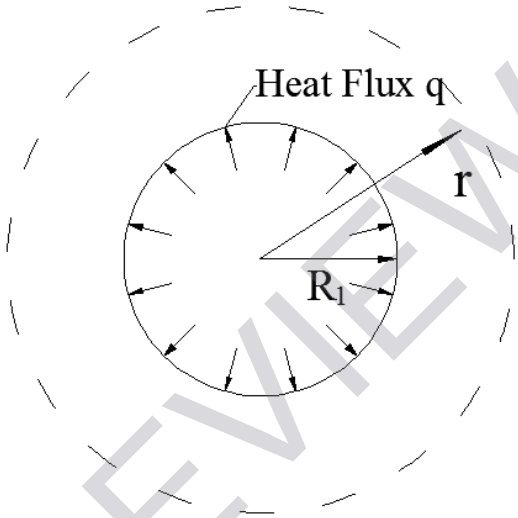

Figure 1a: Geometry for R20 with $R_1 < r < \infty$.

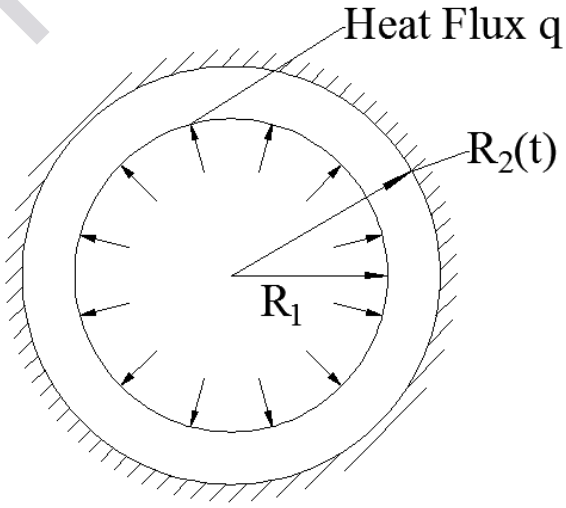

Figure 1b: Geometry for R22 with $R_1 < r < R_2$.

The heat conduction problem for R20 and boundary condition can be expressed by the relations

$$\frac{\partial^2 T(r,t)}{\partial r^2}+\frac{1}{r}\frac{\partial T(r,t)}{\partial r}=\frac{1}{\alpha}\frac{\partial T(r,t)}{\partial t}, \qquad R_1 < r < \infty \qquad (1)$$

$$-k\frac{\partial T}{\partial r}(R_1,t)=q_0 \qquad (2a)$$

$$T(r,0)=T_{in} \qquad (2b)$$

Where the heat flux q_0 is specified on r=R_1.

The general solution can be found by the method of Green's functions [1, Chap8]:

$$T(r,t)=q_0\frac{\alpha}{k}\int_{\tau=0}^{t} G_{20}(r,t|R_1,\tau)2\pi R_1 d\tau \qquad (3)$$

The Green's function of R20 case can be found from [1, p.546]

$$G_{R20}(r,r',t)=\frac{1}{2\pi {R_1}^2}\int_0^{\infty}\frac{\psi(r,\beta)\,\psi(r',\beta)}{[Y_1^2(\beta)+J_1^2(\beta)]}\beta e^{-\beta^2\alpha(t-\tau)/R_1^2}\mathrm{d}\beta \qquad (4)$$

Where:

$$\psi(r,\beta)=J_1(\beta)Y_0(\beta r/R_1)-J_0(\beta r/R_1)Y_1(\beta) \qquad (5)$$

Specifically, For *r=r'=R_1*

$$G_{R20}(R_1,t|R_1,\tau)=\frac{1}{2\pi {R_1}^2}\frac{4}{\pi^2}\int_0^{\infty}\frac{\exp\left[-\frac{\beta^2\alpha(t-\tau)}{{R_1}^2}\right]}{\beta[J_1^2(\beta)+Y_1^2(\beta)]}d\beta \qquad (6)$$

If the dimensionless group applied as:

$$\tilde{T}=\frac{T(r,t)-T_{in}}{\frac{q_0 a}{k}},\tilde{q}=\frac{q(r,t)}{q_0},\tilde{r}=\frac{r}{R_1},\tilde{t}=\frac{\alpha t}{{R_1}^2},\tilde{\tau}=\frac{\alpha\tau}{{R_1}^2} \qquad (7)$$

The dimensionless solution of R20B10T0 can be derived as:

$$\tilde{T}(\tilde{r},\tilde{t})=\int_0^{\tilde{t}}\int_0^{\infty}\frac{\tilde{\psi}(\tilde{r},\beta)\tilde{\psi}(1,\beta)}{[Y_1^2(\beta)+J_1^2(\beta)]}\beta e^{-\beta^2(\tilde{t}-\tilde{\tau})}d\beta d\tilde{\tau}, \qquad 1<\tilde{r}<\infty \qquad (8a)$$

Where:

$$\psi(\tilde{r},\beta) = J_1(\beta)Y_0(\beta\tilde{r}) - J_0(\beta\tilde{r})Y_1(\beta) \qquad (8b)$$

Notice that this result can be simplified by calculating the integral of $\tilde{\tau}$, then the final form of R20's solution can be found as:

$$\tilde{T}(\tilde{r},\tilde{t}) = \int_0^{\infty} \frac{\psi(\tilde{r},\beta)\,\psi(1,\beta)}{[Y_1^2(\beta)+J_1^2(\beta)]}\beta^{-1}(1-e^{-\beta^2\tilde{t}})d\beta, \qquad 1<\tilde{r}<\infty \qquad (9)$$

And the integrand of the solution is:

$$F(\tilde{r},\beta,\tilde{t}) = \frac{\psi(\tilde{r},\beta)\,\psi(1,\beta)}{[Y_1^2(\beta)+J_1^2(\beta)]}\beta^{-1}(1-e^{-\beta^2\tilde{t}}) \qquad (10)$$

In the oil well problem, the wall of well is the location of interest. The dimensionless temperature can be simplified by taking $\tilde{r}=1$ and then the integrand (7) can be simplified as:

$$F(\beta,\tilde{t}) = \frac{\psi(1,\beta)\,\psi(1,\beta)}{[Y_1^2(\beta)+J_1^2(\beta)]}\beta^{-1}(1-e^{-\beta^2\tilde{t}}) \qquad (11)$$

2.2 Numerical integration for R20 case

To get the numerical value for the exact solution of R20 case, Eq. (9) must be integrated numerically and the interval for this integral is from 0 to infinity. To find the most appropriate way to build this numerical integral, the integrand can be plotted with respect to β at different dimensionless times $\tilde{t}$ = 0.5, 1, 5, 10 (shown in legend). From this plot result shown in Fig 2 for $0<\beta<10$, it can be found that the integrand's value goes to 0 for $\beta>10$. What's more, in the integrand there's a term β^{-1} which leads to a singular value at $\beta=0$. However, Fig 2 shows that the integrand is well-behaved at $\beta=0$ (which has a limit of zero). This is due to the term $Y_1^2(\beta)$ approaching infinity as $\beta\to 0$, so the result of $\beta^{-1}/Y_1^2(\beta)$ returns a value $0\times\infty$ which is computationally undefined. In order to deal with these two factors, mid-point rule and improper integral method are needed.

These are discussed in the following sections.

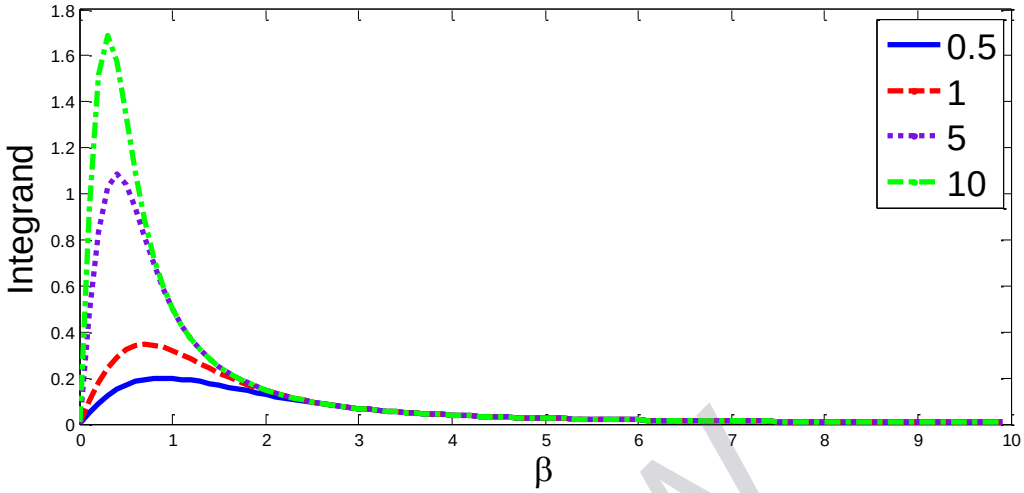

Figure 2: Plot integrand of R20's solution $F(\beta,\tilde{t})$ with $\tilde{t} = 0.5,\ 1,\ 5,\ 10$

2.3 Improper Integral Method for R20 solution

Based on R20 problem, the integral interval is from 0 to infinity which is the improper integral [32]. To evaluate it, break the domain in two pieces:

$$\tilde{T}(\tilde{t}) = \int_0^{\infty} F(\beta,\tilde{t})\,d\beta = \int_0^{b} F(\beta,\tilde{t})\,d\beta + \int_b^{\infty} F(\beta,\tilde{t})\,d\beta, \qquad \tilde{r} = \widetilde{r'} = 1 \quad (12)$$

Where b is an introduced point in integral interval.

And let

$$I_1 = \int_0^{b} F(\beta,\tilde{t})\,d\beta \qquad (13a)$$

$$I_2 = \int_b^{\infty} F(\beta,\tilde{t})\,d\beta \qquad (13b)$$

To convert the improper integral I_2 on (b,∞) to proper integral with finite domain, let $\beta = \frac{1}{z}$, so I_2 can be transformed as:

$$I_2 = \int_0^{\frac{1}{b}} F(\tfrac{1}{z},\tilde{t})\,\tfrac{1}{z^2}\,dz \qquad (13c)$$

This integral has a finite interval so it can be more easily computed than the infinite interval. The new integrand in I_2 can be written as:

$$\bar{F}(z,\tilde{t}) = F(\frac{1}{z},\tilde{t})\frac{1}{z^2} = \frac{\psi\left(\frac{1}{z}\right)\psi\left(\frac{1}{z}\right)}{\left[Y_1^2\left(\frac{1}{z}\right) + J_1^2\left(\frac{1}{z}\right)\right]} z(1 - e^{-\frac{1^2}{z}\tilde{t}})\frac{1}{z^2} \qquad (13d)$$

Figure 3 shows $\bar{F}(z,\tilde{t})$ over z for $\frac{1}{b}=10$. Later in the next section the value of b will be chosen for the best computational behavior. The term $\frac{1}{z^2}$ leads to a singular value at z=0, however the integrand $\bar{F}(z,\tilde{t})$ is well-behaved at z=0 because the term $Y_1^2\left(\frac{1}{z}\right)+J_1^2\left(\frac{1}{z}\right)$ approaches zero for $\frac{1}{z}\to\infty$.

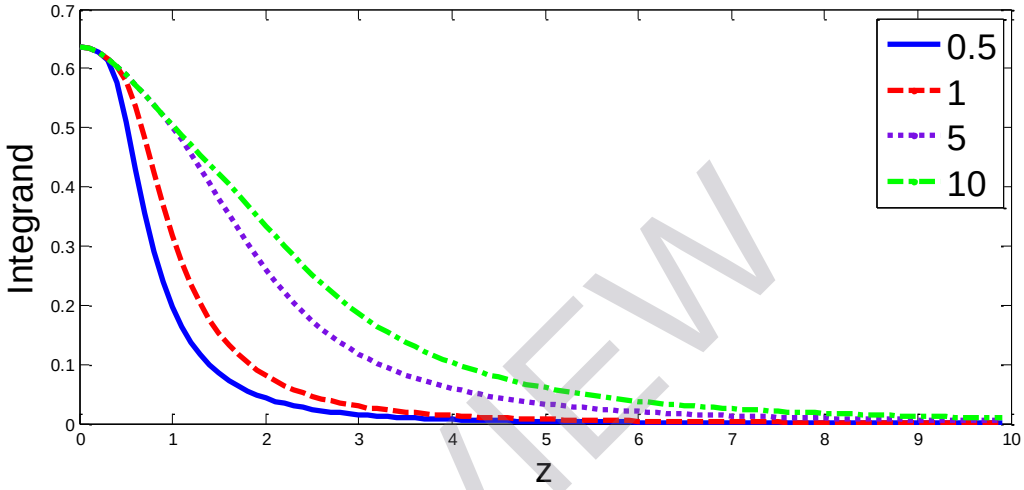

Figure 3: Plot of integrand in improper integral from R20's solution $\bar{F}(z,\tilde{t})$ for 1/b=10 with $\tilde{t}=0.5,\ 1,\ 5,\ 10$

2.4 Mid-Point Rule

It is not possible to evaluate the value of the integrand at $\beta=0$ for both I_1 and I_2. In order to deal with this case, the mid-point mule [33] is the most suitable method of numerical integration. The convergence rate of the mid-point rule is $O(h^2)$. Choosing the upper limit b is another task because it relates to efficiency and accuracy of results. To explore this problem the temperatures were computed at different times at b= *0.1, 0.5, 1, 5*. The number of steps for integrand of I_1 and I_2 is considered as a measure of cost in these calculations. Part of the comparison is shown in Table 1. Table 1 shows that a large number of steps is needed for I_2 at small time at b *=0.1* and for I_1 at large time period at b*=5* to reach the epsilon, but when b*=0.5* and *1* the results have a relative balanced step's numbers as expected, so in this section, b*=1* is selected as the integral limit to compute temperature in numerical integration.

Table 1: Number of computation steps required for temperatures with respect to different time point and separately at *b= 0.1, 0.5, 1, 5.*

ε=10-8, b=0.1				ε=10-8, b=0.5			
time	temp	stepI1	stepI2	time	temp	stepI1	stepI2
0.00001	0.0035492250	104	5076	0.00001	0.0035647652	225	1731
0.0001	0.0111896989	110	1606	0.0001	0.0112334638	225	802
0.001	0.0352062993	109	866	0.001	0.0351914762	225	344
0.005	0.0773794502	109	568	0.005	0.0773843258	225	154
0.01	0.1081034239	109	542	0.01	0.1081034406	225	109
0.05	0.2300535491	110	180	0.05	0.2300672994	227	76
0.1	0.3142337656	110	220	0.1	0.3142347383	228	46
ε=10-8, b=1				ε=10-8, b=5			
time	temp	stepI1	stepI2	time	temp	stepI1	stepI2
0.00001	0.0035647652	278	866	0.00001	0.0035632828	425	344
0.0001	0.0112341528	278	542	0.0001	0.0112341555	425	109
0.001	0.0351914776	278	172	0.001	0.0351913240	426	51
0.005	0.0773837783	278	120	0.005	0.0773838277	430	155
0.01	0.1081026088	279	71	0.01	0.1081027433	435	172
0.05	0.2300672539	282	131	0.05	0.2300674616	466	187
0.1	0.3142343602	286	148	0.1	0.3142346666	492	155

2.5 Comparison between R20 and R22 or R21

In this section the R22 case is studied as a numerically efficient substitution to the R20 case. Compared with R20 case, R22 case has an insulated boundary condition at r=R_2 as shown in Fig 1b. The heat conduction problem for R22 and boundary condition can be expressed by the relations

$$\frac{\partial^2 T(r,t)}{\partial r^2}+\frac{1}{r}\frac{\partial T(r,t)}{\partial r}=\frac{1}{\alpha}\frac{\partial T(r,t)}{\partial t}, \qquad R_1 < r < R_2 \qquad (14)$$

$$-k\frac{\partial T}{\partial r}(R_1,t)=q(t)$$

$$\frac{\partial T}{\partial r}(R_2,t)=0$$

$$T(r,0)=T_{in}$$

Its solution can be found by using Eq. (3) with the R22 Green's function given as